Nuclear Materials and Energy 25 (2020) 100795

Contents lists available at ScienceDirect

Nuclear Materials and Energy

journal homepage: www.elsevier.com/locate/nme

Corrosion behavior of diverse sputtered coatings for the helium cooled pebbles bed (HCPB) breeder concept

T. Hernández [a,*], F.J. Sánchez [a], A. Moroño [a], E. León-Gutiérrez [a], M. Panizo-Laiz [b,c], M. A. Monclus [d], R. González-Arrabal [b,e]

[a] National Laboratory for Magnetic Fusion. CIEMAT. Avda. Complutense 40, 28040 Madrid, Spain
[b] Instituto de Fusión Nuclear "Guillermo Velarde", ETSII, Universidad Politécnica de Madrid (UPM) C/José Gutiérrez Abascal, 2, 28006 Madrid, Spain
[c] Departamento de Física Aplicada e Ingeniería de Materiales, ETSI Industriales, Universidad Politécnica de Madrid, Spain
[d] IMDEA Materiales. Tecnogetafe, 28906 Getafe, Madrid, Spain
[e] Departamento de Ingeniería Energética, ETSI Industriales, Universidad Politécnica de Madrid, José Gutiérrez Abascal, 2, 28006 Madrid, Spain

ARTICLE INFO

Keywords:
Corrosion
HCPB
Coatings: SiC
Al_2O_3

ABSTRACT

The present paper studies the corrosion behavior of several sputtered coatings (nanostructured W, SiC and Al_2O_3) under the working conditions expected for the helium cooled pebbles bed breeder concept to be used in future nuclear fusion reactors. To this purpose, coatings were evaluated during 240 h at a temperature of 550 °C in Helium atmosphere with 120 ppms of water to simulate the purge gas in the presence of ceramic pebbles whose composition was a mixture of lithium silicate/titanate. The 3-D topography, morphology, microstructure and elemental composition of the coatings were studied prior to and after the corrosion tests. Results evidence that coatings show quite different corrosion behavior: Because of oxidation, nW is completely ruled out for such application, the corrosion behavior of Al_2O_3 coating is questionable whereas, SiC coating is shown to act as a real corrosion barrier. Nanoscratch measurements of this last coating show that it also has a good adhesion to the Eurofer substrate both prior to and after the corrosion test.

1. Introduction

The helium cooled pebbles bed (HCPB) is one of the suggested breeder concepts to be used in future fusion nuclear reactors [1]. This design uses ceramic lithium pebbles as breeder, which is especially interesting since pebbles are easier to handle than liquid metals and the associated corrosion problems are much lower than in those concepts considering liquid Li or eutectic 17Li-Pb [2]. However, previous studies indicate that corrosion for bare Eurofer in the HCPB concept is not negligible, especially for long operating times, and indeed it can cause serious problems if not taken into account [3].

One affordable and easy way to overcome this corrosion problem is to cover the steel substrate with a corrosion resistant coating. Such a solution would improve the corrosion behavior of the system (coating/steel) while keeping the structural properties and low cost of the steel. Moreover, coatings are also necessary to prevent tritium leakage [4] allowing a proper and safe reactor operation. Therefore, coating must have two different functions: protect the reduced activation ferritic/martensitic (RAFM) steel against corrosion and, act as a tritium permeation barrier.

Nowadays different methods have been proposed for coatings production such as physical/chemical vapor deposition, thermal spraying, and electrodeposition processes. Because of its properties (easy control, environmental friendly, versatility, scalable and low cost) sputtering is one of the most used techniques for coating fabrication, being the one that we have selected for the materials studies within the present work. Although coating processes are applied to provide the abovementioned benefits, they suffer from disadvantages that degrade their reliability. In particular, for coatings deposited by sputtering the lack of adhesion to the substrate associated to the high compressive residual stresses [5] inherent to the deposition method is a recurring problem [6].

The performance of different coatings (Al_2O_3, TiC, TiC/TiN, W, Au…) as a permeation barrier have been studied [7–9]. In general, experiments performed so far on aluminide and titanium-based ceramic coatings provide high permeation reduction factors, ranging from ~1000 to ~100,000 [10]. The corrosion behavior of some of these layers has been also investigated [11]. However, Most part of reported test were devoted to study the coatings performance on liquid and

* Corresponding author.
E-mail address: teresa.hernandez@ciemat.es (T. Hernández).

https://doi.org/10.1016/j.nme.2020.100795
Received 30 January 2020; Received in revised form 31 August 2020; Accepted 1 September 2020
Available online 8 September 2020
2352-1791/© 2020 The Authors. Published by Elsevier Ltd. This is an open access article under the CC BY-NC-ND license (http://creativecommons.org/licenses/by-nc-nd/4.0/).

eutectic LiPb [12],whereas only few studies deal with the corrosion effects of ceramic lithium pebbles [3].

Based on this knowledge and in our previous experience we have selected sputtered nanostructured W (from now on nW), SiC and Al_2O_3 coatings to check their behavior against corrosion under the presence of ceramic pebbles (mixture of lithium silicate/titanate). This paper is a continuation of a previous one in which the corrosion behavior of different coatings, including Al_2O_3 deposited by pulsed laser deposition and thermal projection, nano-structured tungsten deposited by sputtering and other commercial coatings based on mixed chromium and aluminum oxinitrides fabricated by arc evaporation technique, was evaluated under extreme working conditions (800 °C of temperature, for 730 h in the presence of lithium orthosilicate pebbles). This first work allows us to discard those coatings which do not fulfill minimum requirements [13].

In the present work, we report on the evaluation of the corrosion behavior of several coatings (nanostructured W, SiC and Al_2O_3) deposited by sputtering on Eurofer substrates submitted to 550 °C for 240 h in helium atmosphere with 120 ppms of water to simulate real operation conditions in the presence of ceramic pebbles whose composition was a mixture of lithium **Silicate**/**T**itanate prepared by **K**IT, named in this paper as KST. Firstly, we characterize the topography, morphology, microstructure and elemental composition of the diverse coatings prior to and after the corrosion test. Then, based on these data we discuss about the capabilities and limitation for the different coatings to perform as corrosion barrier. It is worth to mention that in this study, the coating performance as tritium permeation barrier is disregard since it would be further studied for those coatings showing a corrosion resistant behavior. Finally, we have characterized the adhesion of the most promising coating to the Eurofer substrate, since the lack of adhesion would hamper any possible industrial application.

2. Materials and methods

2.1. Coatings deposition

The corrosion behavior of three different coatings (nW, SiC and Al_2O_3) deposited by magnetron sputtering was studied in comparison to that for the bare Eurofer.

All coatings were deposited on polished Eurofer substrates. Polishing was performed by sanding down with F800 and F2400 silicon carbide sandpapers or by 73 mechanical polishing on napless synthetic clothes with a 0.03 μm colloidal alumina suspension.

2.1.1. Nanostructured W (NW) coatings

Nanostructured W (from now on NW) coatings with a thickness of ~4 μm were deposited at the Instituto de Fusión Nuclear "Guillermo Velarde" (IFN-GV). Before introducing the substrates in the deposition chamber, they were cleaned using a sequence of ultrasonic washing with alkaline detergents, rinsing with de-ionized water, cleaning with isopropanol and air-drying. After that, the substrates were introduced in the deposition chamber, where they were further clean by plasma etching in order to remove residual surface contamination. The etching time was 30 min, the DC-pulsed bias voltage was 600 V, the frequency was 150 kHz and the Ar pressure was 6.5×10^{-3} mbar. The deposition setup consists of a high vacuum chamber equipped with a 5 cm diameter magnetron designed and manufactured by Nano4Energy SL [14]. nW coatings were deposited at a normal incidence by combining High Power Impulse Magnetron Sputtering (HiPIMS) and Direct Current Magnetron Sputtering (DCMS). HiPIMS was firstly used to deposit a compliant layer of few hundreds of nanometers to improve the adhesion of the coating to the substrate. HiPIMS deposition took place in DC-pulsed configuration in a pure argon atmosphere at a pressure of 9.5×10^{-3}mbar. The pulse width was 100 μs, the frequency 150 kHz, the peak voltage 450 V, and the plasma current 16 A. Then, the system was immediately set to the DCMS mode. In this mode, the plasma current and the voltage were 0.19 A and 250 V, respectively and, the Ar gas pressure was 8×10^{-3} mbar. The cathode-sample distance was kept constant at 8 cm. More information about the deposition setup and the optimization of tungsten nanostructured coatings can be found in [15]. The NW coatings are made of columns that grow perpendicular to the substrate, presenting an inverted pyramidal shape (compatible with the zone T in the Thornton's morphology diagram [16]). They are pure α-phase, polycrystalline and preferentially oriented along the α-(1 1 0) direction. A more detailed description of the morphological and microstructural properties of the NW coatings is found in Ref. [17,18].

2.1.2. Al_2O_3 coatings

Al_2O_3 coatings with a thickness of 2 μm, were deposited at CIEMAT by reactive magnetron sputtering (RS) working in the DC mode. Coatings were deposited from an aluminum commercial target in the presence of an Ar (85%) + O_2 (15%) atmosphere. Deposition took place in a high vacuum chamber at room temperature. The DC bias of 1.5 kV. The total gas pressure and the target–substrate distance were kept constant at 1.5 $x10^{-1}$ mbar and 4 cm, respectively. After each deposition the Al cathode was cleaned by argon plasma etching to avoid contamination and irreproducibility because of cathode oxidation.

2.1.3. SiC coatings

SiC coatings with a thickness of ~1.5 μm were deposited at the IFN-GV. Before introducing the substrates in the deposition chamber they were cleaned using the same sequence as previously describe for the NW coatings. Then, the substrates were introduced into the deposition chamber and plasma etched using Ar. The etching time was 30 min, the DC-pulsed bias voltage was −350 V the frequency was 150 kHz and the Ar pressure was 5×10^{-3} mbar. The deposition setup consists of a high vacuum chamber equipped with a 5 cm diameter and a rectangular 20 cm × 7.5 cm magnetron; both are designed and manufactured by Nano4Energy SL. Because of thermo-mechanical (quite large differences in the thermal expansion coefficient) incompatibilities between SiC and steel specially when operating at high temperatures, the adhesion of SiC to RAFM steels is difficult. Therefore, based on previous knowledge [19], in order to improve adhesion of the SiC coating to the substrate a Ti interlayer with a thickness of 2 nm was deposited on the bare Eurofer before the deposition of the SiC coating. Ti was deposited by DC magnetron sputtering using the 5 cm diameter magnetron from a pure (99.95%) Ti commercial target at a plasma power of 90 W. Immediately after that and in the same chamber, the SiC coating was deposited by RF magnetron sputtering from a pure (99.95%) SiC commercial target at a plasma power of 300 W. Both depositions took place at a normal incidence angle and at room temperature in the presence of a pure argon atmosphere and at an Ar pressure of 7×10^{-3} mbar. In both cases the target-substrate distance was 10 cm. The sputtered SiC coatings were dense and amorphous.

2.2. Corrosion test

Corrosion test were carried out at CIEMAT by keeping the samples for up to 240 h in direct contact with KST (KIT silicate-titanate) ceramic pebbles formed by a homogenous mixture of Li_4SiO_4 + 20 mol% Li_2TiO_3 prepared at Karlsruhe institute of technology by the KALOS procedure [20]. The temperature during the test was 550 °C. During the test a purge gas consisting of a mixture of He/H_2O (99.8/0.2 %vol) was maintained through the chamber. The addition of a small proportion of water to helium was done to simulate real operating conditions, since it is a better tritium carrier than pure helium. The gas flow was controlled by a screw flowmeter being set to ~1 cm^3/min.

The test setup consists of a special cylindrical chamber with a modular design manufactured at Ciemat which is introduced in a tubular furnace that permits testing temperatures up to 1500 °C. Chamber inner walls are covered with ZrO_2 for protection against corrosion. A more detailed description of this setup is found in ref. [21].

2.3. Characterization methods

The topography of the samples, their morphological and microstructural properties prior to and after the corrosion test were characterized by confocal microscopy, scanning electron microscopy (SEM) and glancing-incident angle (2,5°) X-ray diffraction (GIXRD), respectively. The sample roughness was characterized by interferometry. The elemental composition of the samples prior to and, after the corrosion test was characterized by energy-dispersive X-ray spectroscopy (EDX) and secondary ion mass spectrometry (SIMS).

3D topographic maps were taken by Leica DCM8 confocal microscopy and interferometry system. Scanning electron microscopy/Energy-dispersive X-ray spectroscopy (SEM/EDX) studies were done by using a Zeiss Auriga Compact/Bruker X Flash microscope. GIXRD spectra were measured by using a Philips X-PERT PRO MRD four cycle diffractometer equipped with a CuKα ($\lambda = 0.15405$ nm) radiation source. Secondary ion mass spectroscopy measurements were performed in a Hiden analytical SIMS Workstation.

The adhesion of the coatings with the most promising properties to act as corrosion barriers was quantitatively evaluated by nanoscratch testing. Tests were performed with a Hysitron TI 950 triboindenter using a spheroconical diamond indenter probe with an end radius of 10 μm. Progressive load nanoscratch tests (up to a normal force of 300mN) were carried out while simultaneously recording lateral force and penetration depth. The critical load was determined from the sudden changes in the lateral force and depth data. SEM was used to characterize the failure mode. More than 5 scratch tests separated by 50 μm were carried out on each sample to achieve reproducible and reliable results.

3. Results

A first assessment of the corrosion behavior of the samples can be derived from roughness measurements. Table 1 summarizes the surface roughness prior to and after the corrosion test, together with the thickness of the corrosion layer, if any, for all studied samples.

As illustrated in Table 1, in general, the surface of the as-deposited samples is smooth, being lower than 600 nm in all cases. After corrosion the roughness notably increases for all samples. The largest enhancement (230.8) is observed for the bare Eurofer sample. The corrosion-induced roughness enhancements for the sputtered coatings are much lower than for the bare Eurofer, being 13, 21 and 4.3 for the nW, Al_2O_3 and SiC coatings respectively.

A deeper characterization of the corrosion behavior of the samples is obtained from cross-sectional studies of their morphology, microstructure and elemental composition. In these studies, special attention is paid to lithium depth profiles and to the coating/substrate interface since the loss of adhesion would humper any possible application. In the following, we describe the obtained results for every particular coating. It is worth mentioning that the corrosion behavior of the coatings is studied in reference to that suffered by the bare Eurofer after being exposed to corrosion.

3.1. Bare Eurofer

3D topographic maps prior to and after the corrosion test for the bare Eurofer sample are shown in Fig. 1. The large color contrast observed in this figure for the tested bare Eurofer sample indicates that its surface becomes quite inhomogeneous after the test. Indeed, the imprint left by the KST pebbles on the Eurofer surface is easily seen. This result in agreement with roughness measurements (Table 1) indicate that after the test the surface of the bare Eurofer substrate is highly modified, showing clear effects of corrosion due to the joint action of the temperature and the solid state reaction with the lithium ceramics pebbles.

A cross sectional SEM image and EDX spectra for the tested bare Eurofer samples are shown in Fig. 2a and 2b, respectively. SEM data evidence the presence of a surface layer with a thickness of ~2 μm which is very much affected by corrosion. A closer look to this image in combination with the information provided by EDX and SIMS data (Fig. 3) allows distinguishing that this layer is indeed formed by two layers. One located close to the sample surface with a thickness of ~0.5 μm which is Fe-rich and the other located underneath, with a thickness of ~1.5 μm which is Cr and O-rich. This type of layers has been well described in previous papers in which they have been identified to correspond to an iron oxide of hematite-type and to a mixed oxide of chromium and iron with magnetite structure, respectively [22]. SIMS data depicted in Fig. 3 show that the lithium concentration has a maximum at depths close to the sample surface ($d \leq 500$ nm), then it strongly decreases with increasing depth up to ($d \leq 1.5$ μm); and finally, at depths larger than $d > 1.5$ μm it slightly decreases with depth.

As shown in Fig. 4, XRD spectrum for the tested bare Eurofer exhibits several Bragg peaks corresponding to the hematite-type iron oxide Fe_2O_3 phase. No peaks related to phases containing lithium are observed, however, SIMS data (shown below) show the existence of lithium in that oxide. This means that lithium compounds such as $Li_xFe_{2-x}O_3$ if present, will be amorphous species, as reported in reference [16].

3.2. Nanostructured W (NW) coating

The 3D topography for the NW before and after the corrosion test is shown in Fig. 1. A large color contrast is observed for the tested sample. Light yellow color regions in this image correspond to parts of the sample where NW is still present whereas dark yellow ones are related to bare Eurofer surface after NW has been completely peeled off. This result indicates that the NW coating is partially lost during the corrosion test. In this figure it can be also seen the imprint left by the KST pebbles on the Eurofer surface after coating removal which is an unambiguous sign that corrosion has reached the Eurofer substrate.

Cross-sectional SEM images measured prior and after the corrosion test (Fig. 5a and 5b respectively) taken in the region where the nW coating still remains after the test, show that after the test the nW coating has completely changed. After corrosion, the initial uniform tungsten layer transforms into a thick deposit (with thickness of ~10 μm). Moreover, it is also observed that even in this region the coating is almost detached from the substrate.

Cross-sectional EDX data taken prior and after the corrosion test are shown in Fig. 5. The most relevant information deduce from these data is the notably enhancement observed in the oxygen content along the whole coating depth after being tested. This result would indicate that nanostructured W has been oxidized when being in contact at 500 °C with KST ceramic pebbles in the presence of a He/H_2O gas. It agrees with

Table 1
Surface roughness of the studied samples prior to and after the corrosion test. The roughness is defined as the maximum difference found between the peaks and valleys of the measured linear roughness profiles over the samples. Thickness of the corrosion layer, if any, measured after the test.

Coating	Thickness	Roughness (before corrosion) (μm)	Roughness (after corrosion) (μm)	Standard deviation (μm) (after corrosion)	Corrosion layer thickness
Eurofer (reference)	–	0,13	30	±48	~2 μm
nW	~ 3.5 μm	0.2	2,6	±27	~20 μm
Al_2O_3	~ 2 μm	0.1	2,1	±4	negligible
SiC	~ 1.5 μm	0.6	2,6	±1	negligible

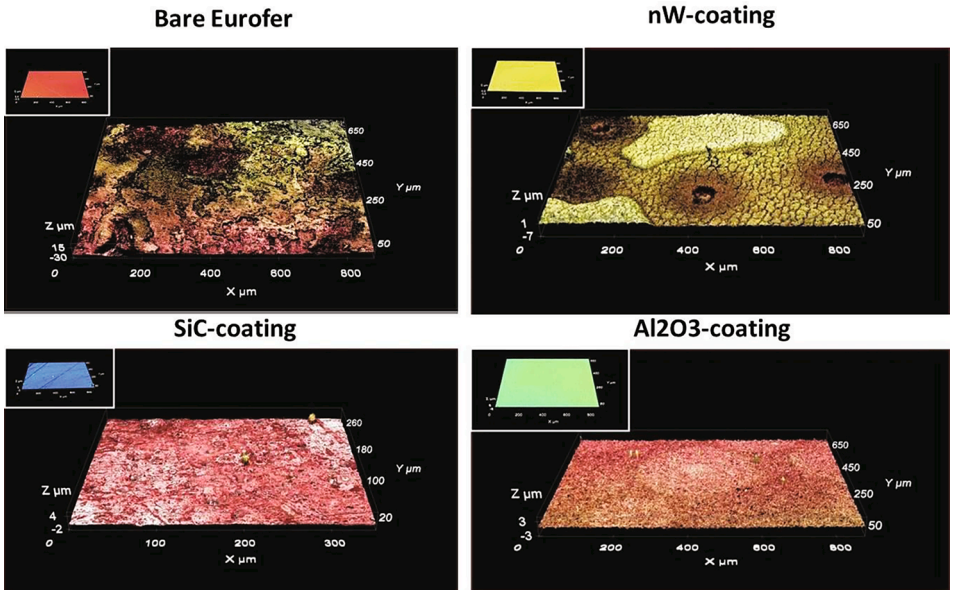


Fig. 1. 3D topographic maps of the of all studied samples prior to (small images in the top left-hand corner) and after the corrosion test (large images).

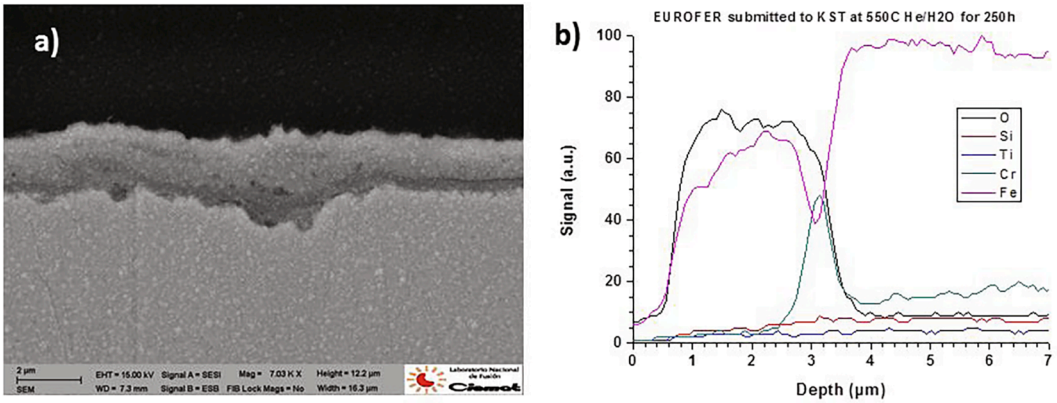


Fig. 2. Cross sectional SEM image (a) and EDX data (b) for bare Eurofer after the corrosion test.

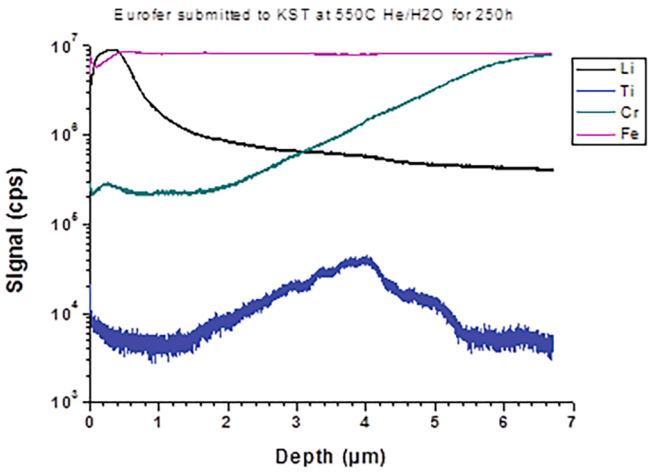


Fig. 3. SIMS spectra for the tested bare Eurofer sample.

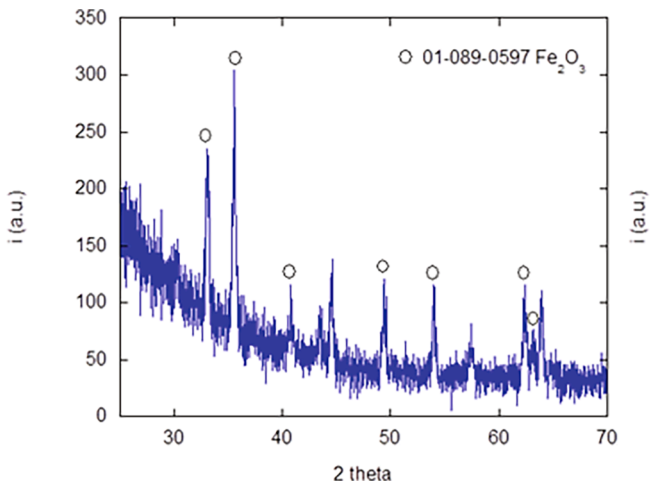


Fig. 4. XRD spectrum for the tested bare Eurofer sample.

that previously reported in which show that the oxidation of W is highly favored in the presence of humidity and that the oxide layers formed are thin at low temperature but grow in thickness at temperatures larger than 300° C [23]. On the other hand, the abnormally high signal for Si can be attributed to debris from the pebbles that are incorporated into the corrosion layer.

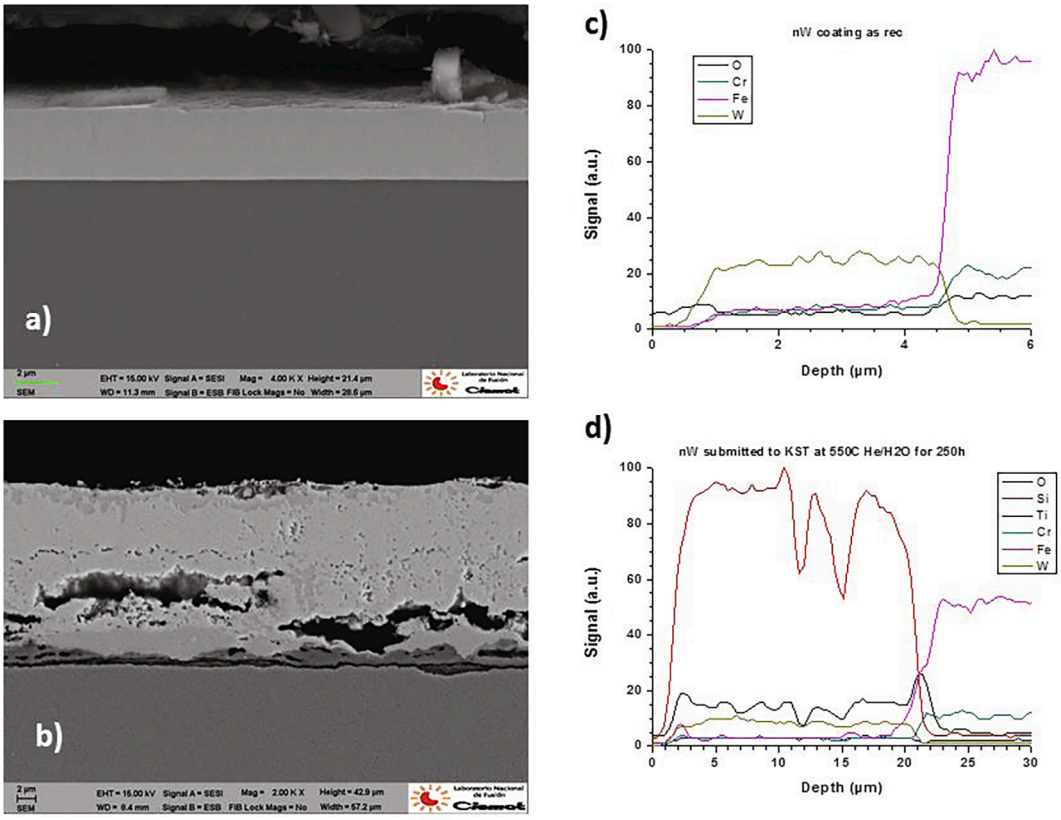


Fig. 5. Cross sectional SEM image for the nW coating prior to (a) and after the corrosion test (b). EDX data for the nW coating prior (c) and after the corrosion test (d).

SIMS data for the as-received and tested coating (Fig. 6a and 6b, respectively) show that the highest Li content is observed at the coating surface and at the coating-substrate interface. Given that the results provided by the SIMS are an average of a 600 × 600 μm area and the layer formed is porous and with loss of material, the Li profile depicted in Fig. 6b shows the addition of different profiles measured in regions still covered by the corrosion layer (high Li content near the surface), regions uncovered with Eurofer exposed directly to the pebbles (high Li content in the interface) and void regions (low Li content), as can be seen in Fig. 5b. On the other hand, the elements Si, Ti and Li are associated with the pebbles, so before exposure in corrosion tests it is considered negligible. Their analysis are not added in the "as received" coatings because it is considered superfluous information that complicates the vision of the figure and provides little value.

XRD spectrum for the tested NW coating depicted in Fig. 7 show several Bragg peaks corresponding to the Fe_2O_3, WO_3, $FeWO_4$ phases. The presence of the WO_3 supporting the EDX data, evidence that the remaining tungsten layer has oxidized. It is important to mention that because of safety reason the formation of this phase is very undesirable, since it is highly volatile and radioactive [24]. Therefore, its formation has to be avoided as much as possible in any imaginable scenario.

The $FeWO_4$ phase can be formed by interaction of WO_3 and FeO at the testing temperature according to the following chemical reaction:

$WO_3 + FeO \rightarrow FeWO_4$,which is thermodynamically stable in the studied temperature range. The observed F_2O_3 phase is also observed in the case of the bare Eurofer, corroborating that after the failure of adhesion, the Eurofer surface is exposed to the corrosion environment without any protection.

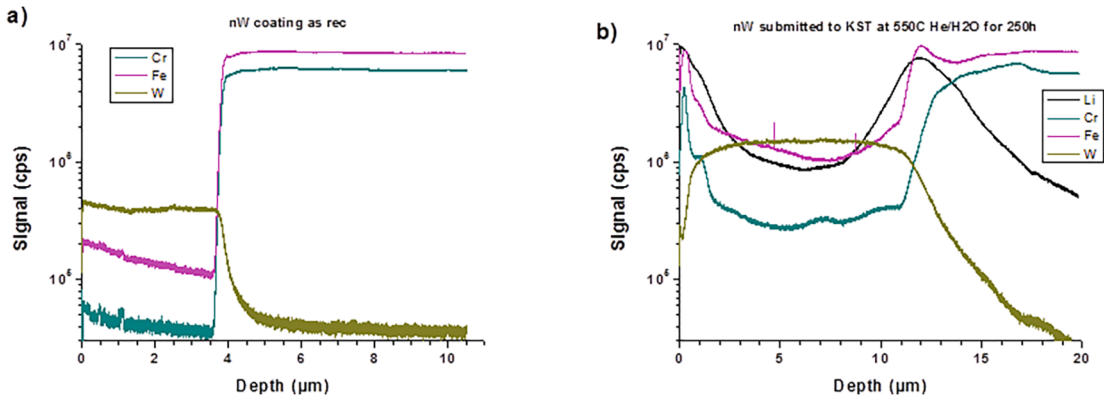


Fig. 6. SIMS spectra for the nW coating measured prior to (a) and after the corrosion tests (b).

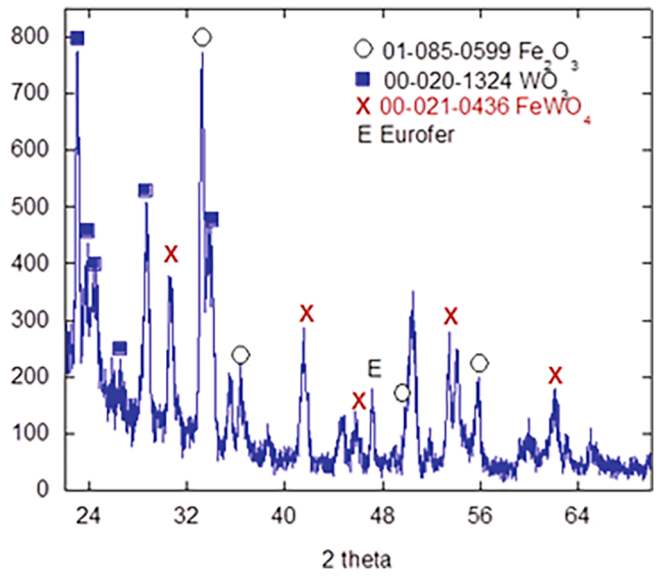


Fig. 7. XRD spectrum for the nW coating after the corrosion test.

3.3. Al_2O_3 coatings

The 3D topography for the Al_2O_3 coating prior to and after the corrosion test is shown in Fig. 1. Both images show a continuous and homogeneous coating surface in combination with cross-sectional SEM images shown in Fig. 8a and b. These results indicate that the test has not been notably modified the morphology of the Al_2O_3 coating along its thickness, but only its surface roughness.

Cross-sectional EDX spectra shown in the same figure for coatings prior to and after the test, respectively, evidence that both coatings have a gradual interface with the substrate since some iron is observed at the substrate/coating interface. SIMS data (Fig. 9) for the tested sample show that lithium homogeneously distributes along the whole coating thickness slightly increasing at the coating-substrate interface. In this case, the analysis also shows the result of different fragments belonging to the aluminum oxide that allow a better detection of the element. These are labeled with the names "AlO, Al2 and Al2O.

XRD pattern for the tested sample depicted in Fig. 10 illustrate that the test has promoted the formation of $LiAlO_2$ due to the solid state reaction taken place between the Al_2O_3 and the small proportions of lithium carbonate or lithium oxide that are always included in the lithium pebbles [25]. Such reactions are reported to happen at temperatures between 400 °C and 1000 °C [26]. Some other phases present in the XRD spectrum corresponds to the Eurofer and to the coating itself.

3.4. SiC coatings

The 3D topography for the SiC coating prior to and after the corrosion test is depicted in Fig. 1. The image shows a continuous and homogeneous coating surface. The low contrast indicates that the surface has not been significantly modified after the test, whereas the small color contrast can be attributed to changes in the surface roughness (see Table 1).

Cross sectional SEM images taken prior to and after the corrosion test are shown in Fig. 11a and 11b, respectively. Apart from a slight modification in the sample surface roughness, no changes are visible in the coating morphology along its thickness. The associated EDX spectra illustrate that as the Al_2O_3 coatings, SiC coatings also have a gradual coating-substrate interface with small presence of Fe in it. This interface became broader after the test which may be related to diffusion processes. SIMS spectra after the test (Fig. 12b) show that lithium is only

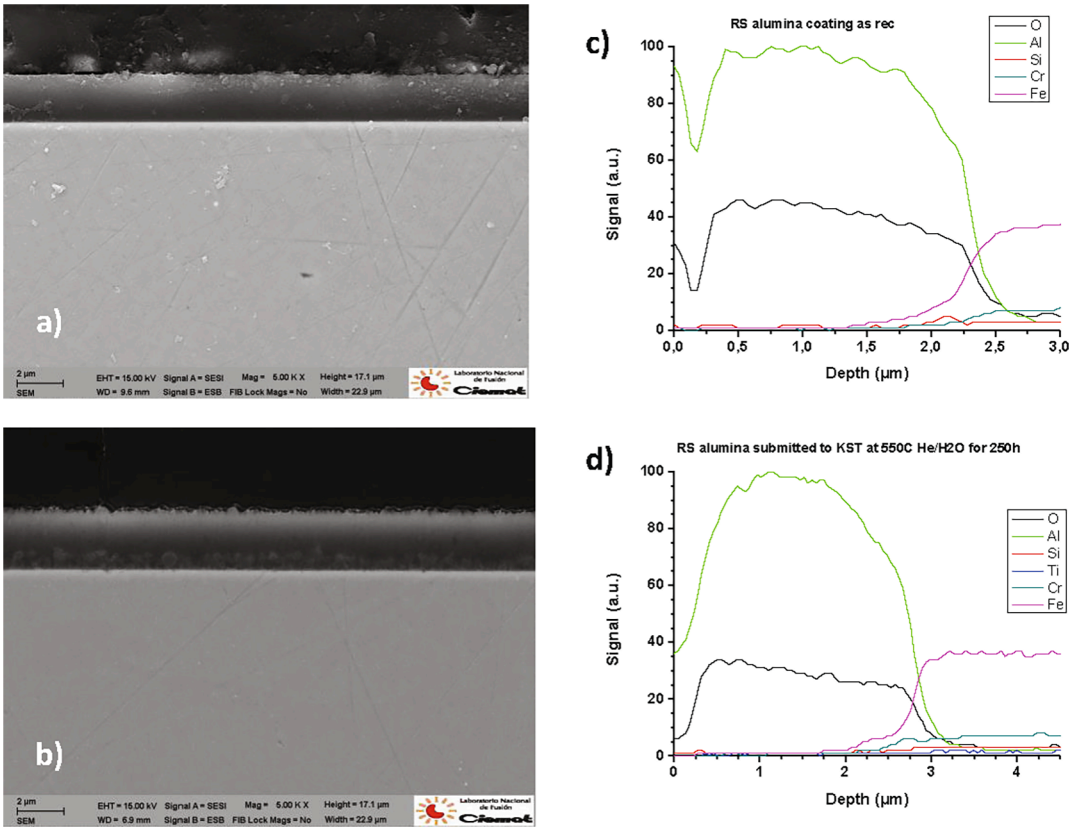


Fig. 8. cross sectional SEM image for the Al_2O_3 coating prior to (a) and after the corrosion test (b). EDX data for the Al_2O_3 coating prior (c) and after the corrosion test (d).

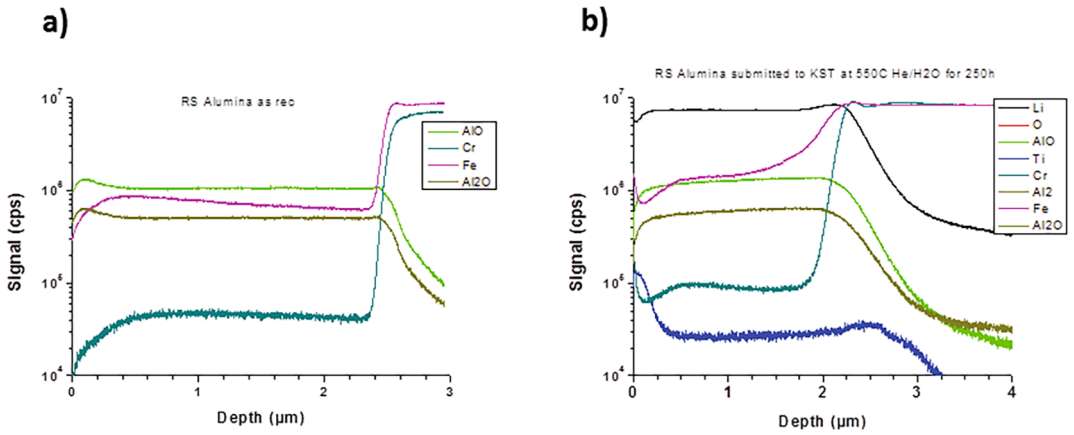


Fig. 9. SIMS spectra for the Al_2O_3 coating measured prior to (a) and after the corrosion tests (b).

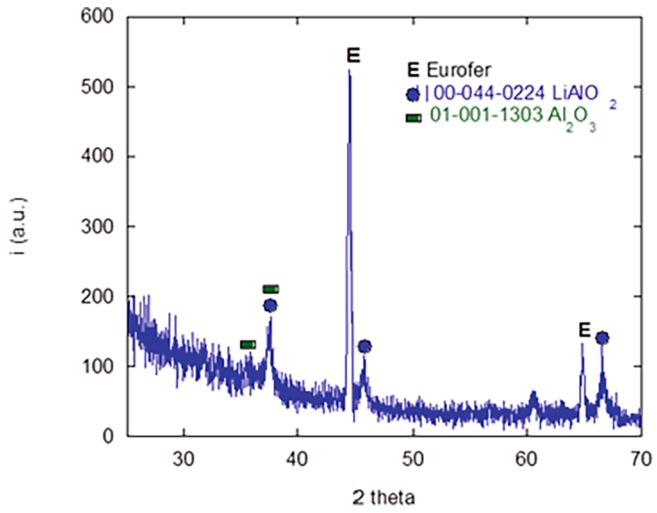


Fig. 10. XRD spectrum for the AL_2O_3 coating after the corrosion test.

observed in a very narrow depth region close to coating surface. No signs of Li are noticed either at the coating-substrate interface or deeper into the substrate, meaning that the SiC coating has fulfilled its protection role. Ti detected at the interface corresponds to the Ti layerdeposited to facilitate adhesion between the SiC and the Eurofer (see section 2.1.3).

The XRD spectra for the tested sample shown in Fig. 13 has two peaks which corresponds to the Fe_3Si phase which, supporting EDX data, indicate the formation of a silicon and iron intermediate phase which is compatible with the gradual coating/substrate interface. No additional phases are observed. These results in agreement with SIMS data evidence the lack of reactivity of SiC with lithium pebbles.

Because of the very good results obtained in the corrosion test, the adhesion of this coating to the substrate has been investigated prior to and after the test, since the lack of adhesion would hamper any possible application of the coating.

Fig. 14a and 14b show representative plots of normal force, normal displacement and lateral force for the SiC sample before and after the corrosion test, respectively.

As shown in Fig. 14a for the as-received SiC coating increasing the lateral displacement leads to a gradual increase in the normal displacement (penetration depth), until it reaches a point where the rate of increase in displacement is faster, which is accompanied by a more unstable lateral force signal. This point is taken as the adhesion failure point and corresponds to normal (critical) load of over 200 mN. On the other hand, the normal displacement signal for the tested SiC coating exhibits a small increase in the normal displacement during the initial 270 nm of lateral displacement, and then a sudden drop, accompanied by a sharp increase of the lateral force signal (Fig. 14b). This point is taken as the adhesion failure point.

The average critical load obtained from at least 8 scratches was 194.5 ± 5.8 mN and 189.5 ± 6.3 mN for the SiC before and after the corrosion test, respectively. The critical load in both cases is very similar, indicating that the effect of the corrosion treatment on the adhesion strength is minimal.

In order to investigate if corrosion has any influence in the failure mode, optical micrographs and detailed SEM images of the scratches were taken. The scratches were done on the sample surface at five different locations that were separated ~70 μm between them in order to have reliable results. Results are shown in Fig. 15a and 15b for the SiC coatings before and after the corrosion test, respectively.

No major chipping or spallation (where the coating flakes off) is observed in and around the scratch track for the as-deposited SiC coating. A detailed view of the secondary electron (SE) image (see Fig. 15a) shows that Hertzian-type circular cracks start to form within the scratch track and also extend over the side of the scratch track. This leads to cohesive spallation along the scratch track borders. The contrast observed in the backscattered electrons (BSE) image illustrated in Fig. 15a reveals changes in the local average atomic number (Z contrast). Therefore, the appearance of brighter areas indicates the presence of a heavier element (Ti) on the surface, meaning that after scratching at that point we have reached the Ti bonding layer (see in Fig. 15a). This is the point taken as representative of coating failure. The whiter areas are more visible as the scratch advances until the coating practically disappears. On the contrary, a more brittle failure mode is observed for the SiC coating after the corrosion test (Fig. 15b). As the scratch advances, conformal type buckling cracks start to appear in the wear track, which eventually leads to sudden large area interfacial coating spallation (adhesive failure) (see in Fig. 15b). This is the point taken as representative of coating failure; prior to this point there is no chipping (no cohesive failure) of the coating, so the failure of the coating in this case occurs abruptly.

3.5. *Lithium diffusion into Eurofer*

When dealing with corrosion barriers a point to be investigated is the lithium inventory at the coating/Eurofer interface and its further penetration into the Eurofer. This is so because the coating-Eurofer interface is a complex area full of defects that can easily accommodate the lithium ions and/or allowing them to further migrate to the Eurofer. Table 2 summarizes the lithium diffusion coefficients in Eurofer obtained from SIMS data assuming a simple diffusion process. On this basis, the amount of lithium transferred to the Eurofer can be fitted using the complementary error function:

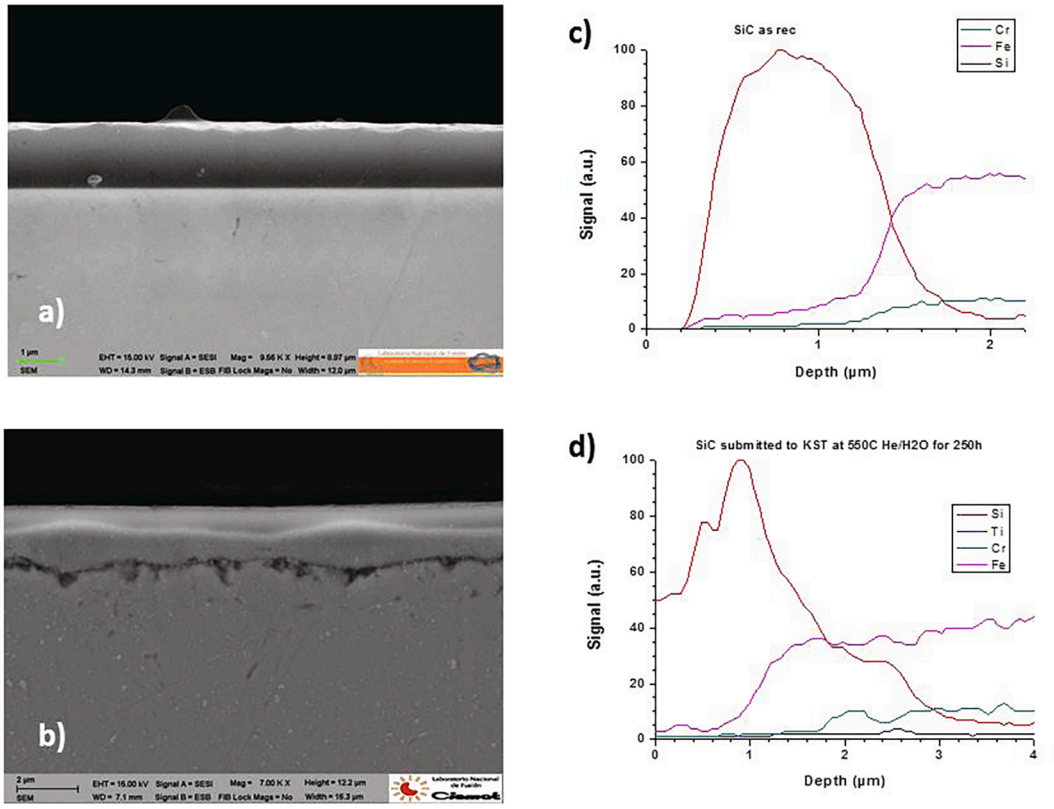


Fig. 11. Cross sectional SEM image for the SiC coating prior to (a) and after the corrosion test (b). EDX data for the SiC coating prior (c) and after the corrosion test (d).

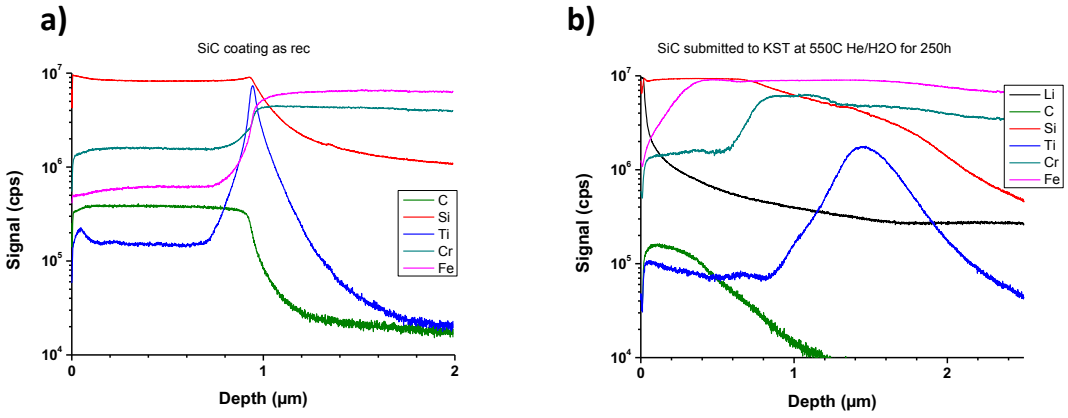


Fig. 12. SIMS spectra for the SiC coating measured prior to (a) and after the corrosion tests (b).

$$C = C_o erfc\left(\frac{x}{2\sqrt{Dt}}\right)$$

where Co is the number of counts per second detected for the studied element (Li) in the surface, and D and t are the effective diffusion coefficient (cm2/s), and heating period (s), respectively.

The diffusion coefficients for the different coatings are listed in Table 2. Here, notable differences for the diverse coatings are observed. These dissimilarities in data can be associated to the different interfaces. For the bare Eurofer, it has been observed that the lithium completely crosses the corrosion bilayer and it introduces into the chromium depleted region of the Eurofer. From now on, this value will be considered as a reference. The diffusion coefficient for the NW coating is much higher than the reference value meaning that the NW coating far from protecting steel, favors its higher damage. This can be associated to the coating degradation promoted by the oxidation of W under the test conditions and the Li reactivity; the combine effect of both things would provide a porous interface in which Li can easily move. The penetration of lithium for the NW coating is almost four times higher than that for the bare Eurofer.

The diffusion coefficient for the SiC and Al_2O_3 coatings are significantly lower than that for the bare Eurofer. The lowest diffusion coefficient ($1x10^{-17}$ cm^2/s) is found for the SiC coating, approximately 100 times less than that for the bare Eurofer. This is so because SiC is a stable material with exceptionally low chemical reactivity which is able to prevent the lithium transfer to the interface and, therefore, its further penetration into the Eurofer.

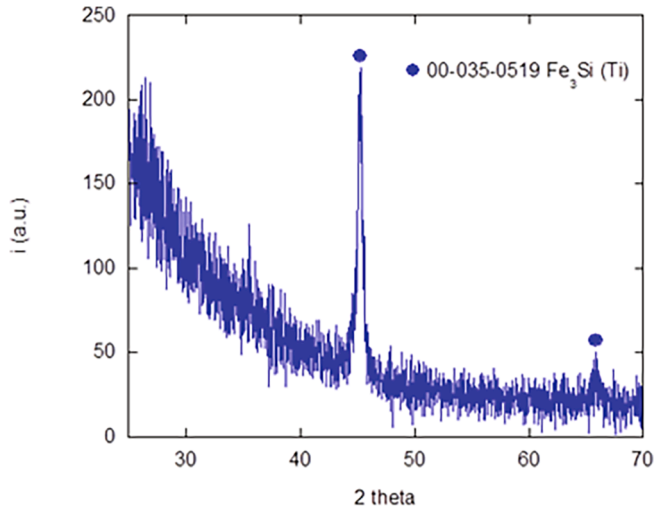


Fig. 13. XRD spectrum for the SiC coating after the corrosion test.

4. Discussion

The present work provides important information about the capabilities and limitations of different coatings to act as corrosion barriers for the HCPB breeder concept.

Because of oxidation, the NW coating transform into WO_3. The W oxidation would be the responsible for the increases in thickness measured after the corrosion test. These two facts could be the reason for the loss of adhesion of the coating to the substrate. Therefore, the NW does not satisfactorily withstand the corrosion test, since it has not fulfilled its protection role for the Eurofer.

Al_2O_3 coatings do not act as real barriers since lithium has been found all along the coating thickness and penetrating into the Eurofer substrate underneath. This presence of lithium in the Al_2O_3 under the testing condition has favored the formation of the $LiAlO_2$ phase due to the solid state reaction occurring at the test temperatures. Such reaction would initiate at the coating surface but eventually it could diffuse until the alumina structure is saturated in lithium. The fact that the measured lithium content is constant along the whole coating thickness supports this hypothesis. The lithium diffusion along the Al_2O_3 coatings is a complex process which depends, among other factors, on the crystalline structure of the coating as well as, on its density. In our particular case, since the Al_2O_3 coatings we are dealing with is, in no case a ceramic material with a typical polycrystalline microstructure of grains and grain boundaries, we assume that the low density of the Al_2O_3 coatings and its mostly amorphous state (extremely small and not crystalline particles, which occasionally present crystalline domains of short scope) are the factors favoring the transport of lithium. The fact that the Al_2O_3 coating is lithium saturated in only 240 h, allows lithium to accumulate at the coating-substrate interface which damages the steel surface to a greater extent. The analysis of the steel damage due to the accumulation of lithium at the interface and its transfer within the Eurofer needs to be evaluated in more detail. The worst imaginable situation is that irradiation of lithium with neutrons favors the formation of helium bubbles that will deteriorate the mechanical properties of the structural material [27]. But, this does not necessarily have to happen, since it depends among other factors on the weight factors such as the neutron flux received and the scope of lithium in the Eurofer long term. A detailed study of this subject falls out of the scope of the present study.

SiC has satisfactorily withstood the corrosion test, acting as a real barrier to lithium and protecting the Eurofer against corrosion. This is so because SiC in all its crystalline phases and allotropic forms is extremely inert in contact with the lithium pebbles. Moreover, studied SiC coatings have a good adhesion to the Eurofer substrate both prior to and after the corrosion test. Indeed, after the test only a small decrease in the critical load is observed. All data evaluated here point that it is a good candidate for the HCPB breeder concept. However, a complete material qualification would require studying its behavior as a tritium permeation barrier. Previous reported permeation studies reported so far SiC coatings deposited by different methods [28–30], show that SiC is an excellent barrier for preventing the permeation of hydrogen isotopes. Nevertheless, because of the dependence of the hydrogen-isotope diffusivity of SiC on crystallinity, phase, morphology, and impurity content [31], and because of the influence of the sputtering parameters on the coating morphology and microstructure [32], a proper characterization of the permeation behavior of the SiC coatings studied here would be necessary. This would be the subject of a future work.

5. Conclusions

The corrosion produced in the bare Eurofer being in contact with ceramic pebbles should not be neglected. Although it is not comparable to the one observed for the Eurofer submitted to tests that handle PbLi, especially at high flow rate, it can alter the bare material and be strongly relevant under irradiation.

Because of oxidation and its derived problems, the use of NW for the protection against corrosion in the HCPB conditions is ruled out.

The use of Al_2O_3 coatings as corrosion barriers is still unclear, since the solid state reaction taken place between the Al_2O_3 coatings and the

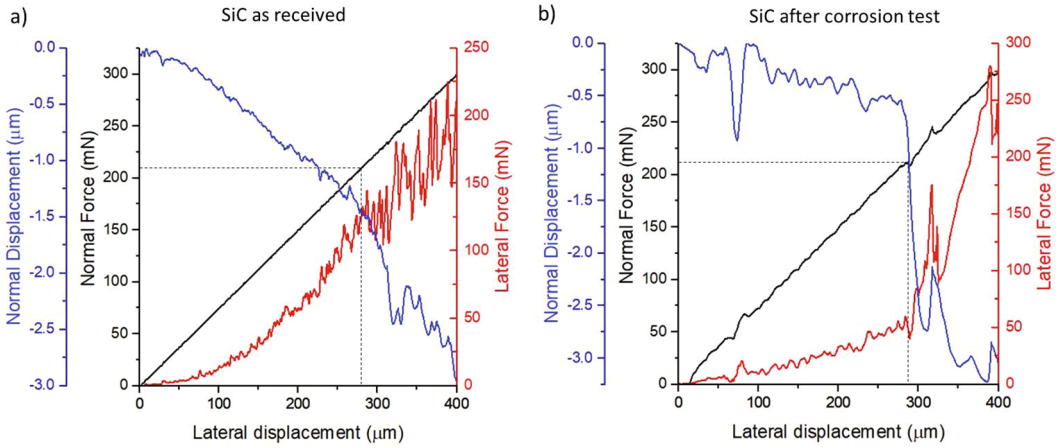


Fig. 14. Evolution of the normal force (black), lateral force (red) and normal depth (blue) with the lateral displacement for the SiC coatings before (as received) (a) and after the corrosion test (b).

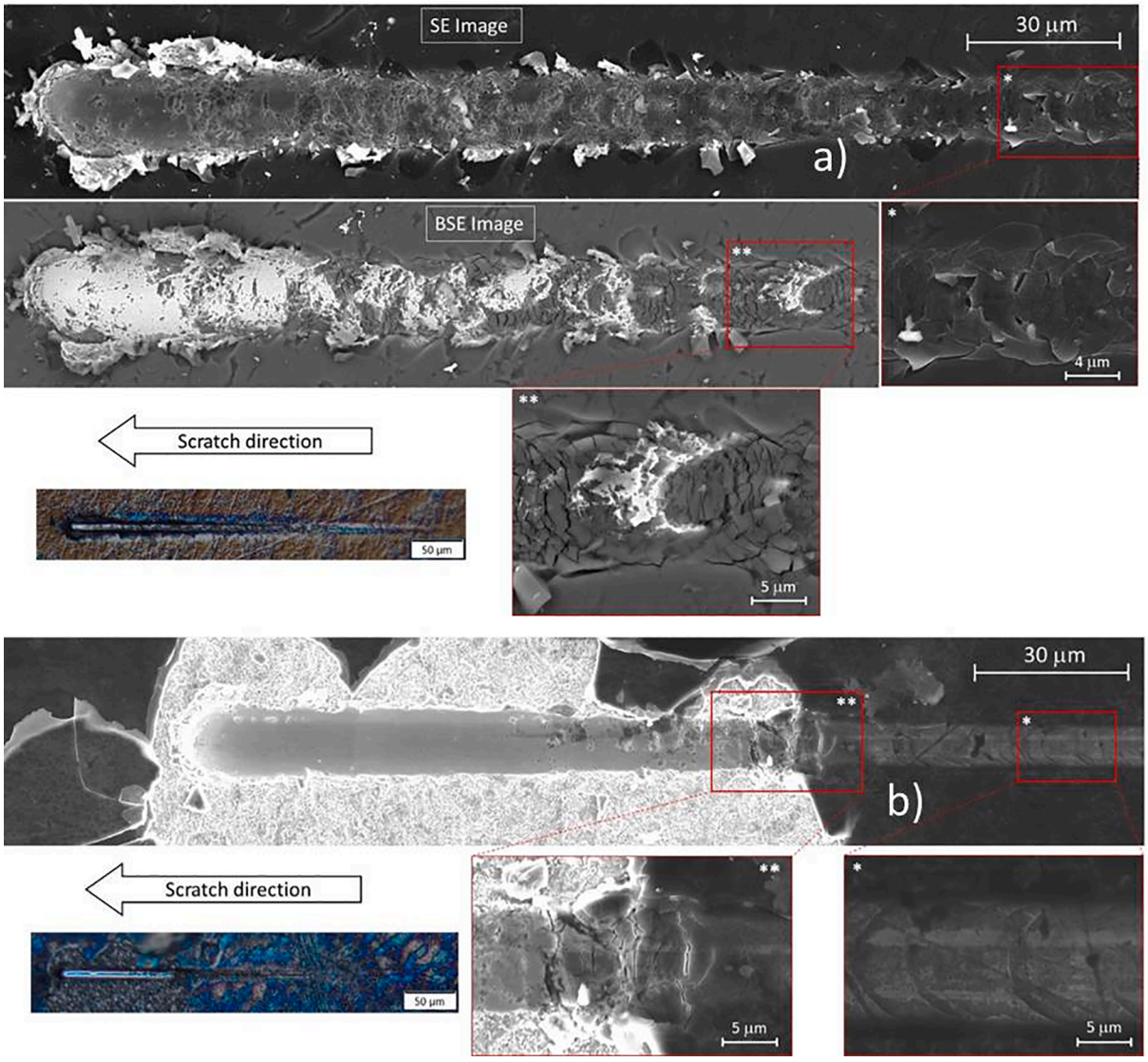


Fig. 15. (a) SEM images and optical micrographs of the scratch tracks for the SiC coatings prior to the corrosion test. (b) SEM images and optical micrographs of the scratch tracks for the SiC coatings after the corrosion test.

Table 2
Diffusion coefficients obtained by fitting the experimental data using the complementary error function.

Coating	Diffusion coefficient (cm^2/s)	R:Dc/Dr
Eurofer (reference)	0.95×10^{-15}	1
NW	3.5×10^{-14}	3.7
Al_2O_3	9×10^{-16}	0.1
SiC	1×10^{-17}	0.01

ceramic pebbles containing lithium leads to the formation of $LiAlO_2$ allowing the penetration of Li into the coating, through the whole coating up to first layers of the Eurofer substrate underneath. The implications of this lithium diffusion in the capabilities of the Al_2O_3 coatings as corrosion barriers should be further investigated. It is also important to mention that under the studied corrosion conditions the lithium permeation through the Al_2O_3 coatings has been observed to depend on the coating density and microstructure, being lower for dense and well-ordered coatings. Therefore, future efforts would be oriented to study the anticorrosion properties of Al_2O_3 coatings as a function of sputtering parameters to optimize them.

SiC coatings have been demonstrated to be a stable material with exceptionally low chemical reactivity with lithium. Therefore, SiC emerges as a promising material acting as a real barrier to lithium and protecting the Eurofer against corrosion. Moreover, these coatings have a good adhesion to the substrate, even after the corrosion test.

In conclusion, of all the investigated coatings (nW, Al_2O_3 and SiC), SiC seems to be the most promising one to act as a corrosion barrier. Future work would require characterizing behavior of these coatings as tritium permeation barriers.

CRediT authorship contribution statement

T. Hernández: Conceptualization, Supervision, Writing - original draft, Investigation. **F.J. Sánchez:** Investigation, Methodology. **A. Moroño:** Investigation, Methodology. **E. León-Gutiérrez:** Validation. **M. Panizo-Laiz:** Investigation, Methodology. **M.A. Monclus:** Investigation, Methodology. **R. González-Arrabal:** Investigation, Writing - review & editing.

Declaration of Competing Interest

The authors declare that they have no known competing financial interests or personal relationships that could have appeared to influence

the work reported in this paper.

Acknowledgements

This work has been carried out within the framework of the EUROfusion Consortium and has received funding from the Euratom research and training programme 2014-2018 and 2019-2020 under grant agreement No 633053. The views and opinions expressed herein do not necessarily reflect those of the European Commission.“ This work has been supported by MICIU Project (Ministerio de Ciencia, Innovación y Universidades) PID2019-105325RB-C31 and TechnoFusion Project (P2018/EMT-4437) of the CAM (Comunidad Autónoma Madrid). The authors wish to thank M. Martín, J.M. García, J. Valle and F. Jiménez for their help in the experiments.

References

[1] F. Hernández, P. Pereslavtsev, Q. Kang, P. Norajitra, B. Kiss, G. Nádasi, O. Bitz, A new HCPB breeding blanket for the EU DEMO: evolution, rationale and preliminary performances, Fus. Eng. Design 124 (2017) 882–886.
[2] J. Konys, W. Krauss, H. Steiner, J. Novotny, A. Skrypnik, Flow rate dependent corrosion behavior of Eurofer steel in Pb–15.7Li, J. Nucl. Mat. 417 (2011) 1191–1194.
[3] K. Mukai, F. Sanchez, R. Knitter, Chemical compatibility study between ceramic breeder and EUROFER97 steel for HCPB-DEMO blanket, J. Nucl. Mater. 488 (2017) 196–203.
[4] F. Franza, L.V. Boccaccini, A. Ciampichetti, M. Zucchetti, Tritium transport analysis in HCPB DEMO blanket with the FUS-TPC code, Fus. Eng. Design 88 (2013) 2444–2447.
[5] J.A. Thornton, Internal stresses in titanium, nickel, molybdenum, and tantalum films deposited by cylindrical magnetron sputtering, J. Vacuum Sci. Tech. 14 (1977) 164–169.
[6] K. Bobzin, T. Brögelmann, C. Kalscheuer, M. Engels, Synthesis of a-C coatings by HPPMS using Ar, Ne and He as process gases, Surf. Coat. Technol. 308 (2016) 80–89.
[7] Vincenc Nemanic, Hydrogen permeation barriers: basic requeriments, materials selection, deposition methods and quality evaluation, Nucl. Mater. Energy 19 (2019) 451–457.
[8] A. Perujo, K.S. Forcey, Tritium permeation barriers for fusion technology, Fus. Eng. Design 28 (1995) 252–257.
[9] R. Frauenfelder, Permeation of hydrogen through Tungsten and molybdenum, J. Chem. Phys. 48 (1968) 3955–3960.
[10] G.W. Hollenberg, E.P. Simonen, G. Kalinin, A. Terlain, Tritium/hydrogen barrier development, Fus. Eng. Design 28 (1995) 190–208.
[11] Lu. Wei, Jing Wang, Pu. Wenjing, Kaiping Li, Weihua Wang, Shengnan He, Delin Chu, Jinhong Yang, Yuhao Zhu, Corrosion resistance of ceramic candidates for tritium permeation barriers exposed to molten lithium, Corros. Sci. 160 (2019) 108172–108176.
[12] H. Glasbrenner, J. Konys, Z. Voss, O. Wedemeyer, Corrosion behaviour of Al based tritium permeation barriers in flowing Pb–17Li, J. . Nucl. Mat. 307–311 Part. 2 (2002) 1360–1363.
[13] T. Hernández, F.J. Sánchez, F. Di Fonzo, M. Vanazzi, M. Panizoc, R. González-Arrabal, Corrosion protective action of different coatings for the helium cooled pebble bed breeder concept, J. Nucl. Mater 516 (2019) 160–168.
[14] https://nano4energy.eu/.
[15] N. Gordillo, C. Gómez de Castro, E. Tejado, J.Y. Pastor, G. Balabanian, M. Panizo-Laiz, R. Gonzalez-Arrabal, J.M. Perlado, J. del Rio, On the thermal stability of the nanostructured tungsten coatings, Surf. Coat. Tech. 325 (2017) 588–593.
[16] J.A. Thornton, Influence of substrate temperature and deposition rate on structure of thick sputtered Cu coatings, J. Vac. Sci. Technol. 12 (1975) 830–836.
[17] N. Gordillo, M. Panizo-Laiz, E. Tejado, I. Fernandez-Martinez, A. Rivera, J. Y. Pastor, C. Gómez de Castro, J. del Rio, J.M. Perlado, R. Gonzalez-Arrabal, Morphological and microstructural characterization of nanostructured pure α-phase W coatings on a wide thickness range, Appl. Surf. Sci. 316 (2014) 1–8.
[18] N. Gordillo, M. Panizo-Laiz, E. Tejado, I. Fernandez-Martinez, A. Rivera, J. Y. Pastor, C.G. de Castro, J. del Rio, J.M. Perlado, R. Gonzalez-Arrabal, Morphological and microstructural characterization of nanostructured pure α-phase W coatings on a wide thickness range, Appl. Surf. Sci. 316 (2014) 1–8.
[19] Zhihong Zhong, T. Hinoki, A. Kohyama, Microstructure and mechanical strength of diffusion bonded joints between silicon carbide and F82H steel, J. Nucl. Mater. 417 (2011) 395–399.
[20] R. Knitter, M. Kolb, U. Kaufmann, A. Goraieb, Fabrication of modified lithium orthosilicate pebbles by addition of titania, J. Nucl. Mater. 442 (2013) S433.
[21] T. Hernández, M. Carmona Gázquez, F.J. Sánchez, M. Malo, Corrosion mechanisms of Eurofer produced by lithium ceramics under fusion relevant conditions, Nucl. Mater. Energy 15 (2018) 110–114.
[22] T. Hernández, P. Fernández, Corrosion susceptibility comparison of EUROFER steel in contact two lithium silicate breeders, Fus. Eng. Design 89 (7–8) (2014) 1436–1439.
[23] A. Warren, A. Nylund, I. Olefjord, Oxidation of tungsten and tungsten carbide in dry and humid atmospheres, Int. J. Refract Metals Hard Mater. 14 (5–6) (1996) 345–353.
[24] G.R. Smolik, S.J. Piet, R.M. Neilson Jr., Predictions of radioactive Tungsten release for hypothetical ITER accidents, Fusion Technol. 19 (3P2B) (1991) 1398–1402.
[25] D. Mandal, M.C. Jadeja, B.K. Chougule, Synthesis of lithium orthosilicate and fabrication of pebbles by the solid-state reaction process, Indian Chem. Eng. 59 (1) (2017) 21–30.
[26] Y. Ikeda, H. Ito, G. Matsumoto, H. Hayashi, Thermal stability of lithium aluminates by high temperature mass spectrometry, J. Nucl. Sci. Tech. 17 (8) (1980) 650–653.
[27] M.J. Demkowicz, A. Misra, A. Caro, The role of interface structure in controlling high helium concentrations, current opinion in sol, State Mater. Sci. 16 (3) (2012) 101–108.
[28] R.A. Causeya, W.R. Wamplerb, The use of silicon carbide as a tritium permeation barrier, J. Nucl. Mater. 220–222 (1995) 823–826.
[29] P. Muñoz, T. Hernández, I. García-Cortés, F.J. Sánchez, A. Maira, D. Iadicicco, M. Vanazzi, M. Utili, F. Di Fonzo, A. Moroño, Radiation effects on deuterium permeation for PLD alumina coated Eurofer steel measured during 1.8 MeV electron irradiation, J. Nucl. Mater. 512 (2018) 118–125.
[30] R. Checchetto, L.M. Gratton, A. Miotello, Hydrogen permeation in I amorphous-SW stainless steel bilayers, Phys. D: Appl. Phys. 27 (1994) 1687–1690.
[31] G.M. Wright, M.G. Durrett, K.W. Hoover, L.A. Kesler, D.G. Whyte, Silicon carbide as a tritium permeation barrier in tungsten plasma-facing components, J. Nucl. Mater. 458 (2015) 272–274.
[32] Takumi Chikada, Akihiro Suzuki, Takayuki Terai, Deuterium permeation and thermal behaviors of amorphous silicon carbide coatings on steels, Fus. Engi. Design 86 (9–11) (2011) 2192–2195.